Growth Mechanisms of Vertically-aligned Carbon, Boron Nitride, and Zinc Oxide Nanotubes

Yoke Khin Yap

Department of Physics, Michigan Technological University, 118 Fisher Hall, 1400 Townsend Drive, Houghton, MI 49931, U.S.A.

Abstract. Nanotubes are one-dimensional nanomaterials with all atoms located near the surface. This article provides a brief review on the possible growth mechanisms of a series of inorganic nanotubes, in particular, vertically-aligned (VA) carbon nanotubes (CNTs), boron nitride nanotubes (BNNTs), and ZnO nanotubes (ZnO NTs).

Keywords: Carbon Nanotubes, Boron Nitride Nanotubes, Zinc Oxide Nanotubes, Silicon Nanotubes

INTRODUCTION

Inorganic nanotubes are structurally unique with all their atoms located near the surface. Electron flows on nanotubes are thus confined near the surface and can be modulated by charge transfers from or to foreign molecules attached on nanotubes. Therefore, nanotubes are attractive materials for chemical and biological sensing. Because of the tubular structures, nanotubes are also applicable nanoscale fluidic devices. We classify inorganic nanotubes into two categories: 1) atomically seamless nanotubes, and 2) artificial nanotubes. Carbon nanotubes (CNTs) [1-3] and boron nitride nanotubes (BNNTs) [4, 5] representing the first type of nanotubes, ideally, with no dangling bonds even at the surfaces of the nanotubular structures. This type of nanotubes has no bulk precursor that sharing the same crystal structure. On the other hand, artificial nanotubes are having the same crystallographic properties as their bulk precursors, for example, zinc oxide nanotubes (ZnO NTs) [6-8] are having and silicon nanotubes (SiNTs) [9, 10]. Unlike CNTs and BNNTs, atoms at the surface of artificial nanotubes are not saturated with chemical bonds and thus readily functionalization with other molecules and atoms for achieving property modification. Because of the page limit, this article provides a brief summary on the possible growth mechanisms of vertically-aligned CNTs [11-13], BNNTs [14, 7], and ZnO NTs [6-8]. Readers are encouraged to refer to the related references for SiNTs and more comprehensive description on CNTs, BNNTs, and ZnO NTs.

CP1150, *Frontiers in Physics – 3rd International Meeting,* edited by S.-P. Chia, M. R. Muhamad, and K. Ratnavelu

VERTICALLY-ALIGNED CARBON NANOTUBES

Catalytic thermal chemical vapor deposition (CVD) is a convenient technique for growing CNTs. The well-accepted vapor-liquid-solid (VLS) growth mechanism involves the decomposition of hydrocarbon gases on the catalytic nanoparticles, the diffusion of carbon into the catalyst until saturation, and subsequent segregation of carbon from the catalyst as nanotubes. However, the VLS model does not provide sufficient details on the decomposition process of the hydrocarbon molecules on the catalytic nanoparticles.

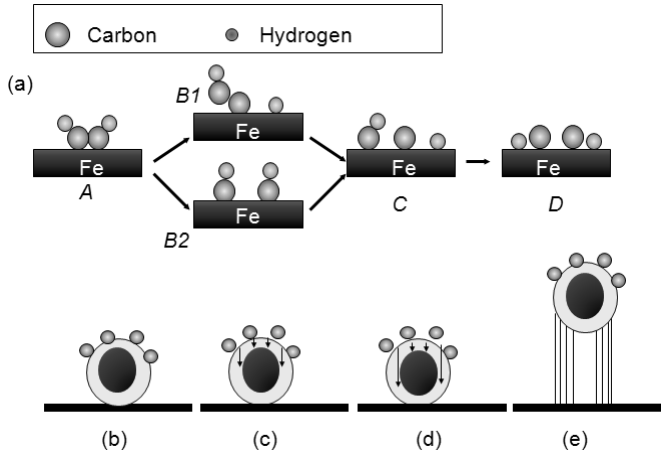

FIGURE 1. (a) Sequences of dissociative adsorption of C_2H_2 on Fe surface. See text for detailed description. The (b) decomposed carbon atoms (c) diffused into the solid-core Fe nanoparticle until (d) supersaturation and then (e) segregate as nanotubes.

In fact, the catalytic decomposition process is known as dissociative adsorption. Figure 1 illustrates a growth model that combined the details of dissociative adsorption and the VLS mechanism [see [13] for more comprehensive references]. Figure 1a shows the adsorption of acetylene (C_2H_2) molecules (step *A*) on the surface of the catalytic Fe nanoparticles. This will lead to either the breaking of C-H bond (step *B1*) to form C_2H and H fragments or the breaking of C=C bond (step *B2*) to form two C-H fragments. The catalytic function of the Fe nanoparticles is to reduce the energy required for decomposition by a charge transfer from hydrocarbon molecules to Fe. According to a first principles calculation, the dissociation energy of the first hydrogen atom from an isolated C_2H_2 (step *A* to *B1*) in vacuum can be reduced from 5.58 eV to 0.96 eV. On the other hand, the energy barrier between *A* and *B2* is 1.25 eV. The C-H bond breaking (step *B1*) is followed by C-C bond breaking (step *C*) with a potential barrier of 1.02 eV. Whereas, C=C bond breaking (step *B2*) is followed by C-H bond breaking (step *C*) with an energy barrier of 0.61 eV. Both modes (*A* to *B1* to *C or A* to *B2* to *C*) are possible and give one C-H fragment, one C and one H. The decomposition of C_2H_2 is completed after the breaking of the last C-H bond (step *D*) with the need of a potential energy of 0.61 eV.

The decomposed carbon atoms (Figure 1b) will then diffuse into the Fe nanoparticles (Figure 1c). At typical growth temperature (650-800 ^{o}C), these

nanoparticles are not melted even after considering the eutectic point of Fe-C phase [15]. Since dissociative adsorption is an exothermic process, the near surface temperatures of the catalytic nanoparticles will be higher than the growth temperatures. Since the melting of nanoparticles starts from their surfaces [16], it is possible that the near surface region of the particles is melted. This will form the gas-liquid interface between carbon and Fe solid-core nanoparticles. Due to the high diffusion rate of carbon in Fe melt, a Fe-C alloy will start to form. When these nanoparticles become supersaturated with carbon (Figure 1d) to a value critical for growth at the solid-liquid interface, the excess carbon will segregate as carbon nanotubes (Figure 1e). A tip-growth mode is illustrated in this figure where the nanoparticles remained at the tips of CNTs. A base-growth mode is also possible where the nanoparticles remained at the bases of CNTs.

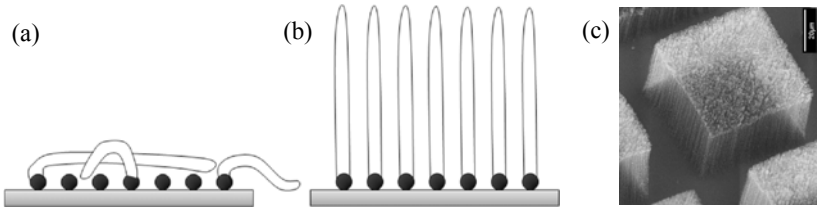

FIGURE 2. (a) CNTs grown in (a) random mode and (b) vertically-aligned mode. (c) Bundles of CNTs grown on patterned catalysts.

Figure 2 shows the difference between random growth mode and vertically-aligned growth mode of CNTs. For cases where the density of effective catalyst (Fe nanoparticles in our case) is not high, CNTs are free to grow in all directions and tend to rest and stack on the substrate surface randomly (Figure 2a). For cases with high density of active catalysts, every nanotubes will be surrounded by adjacent nanotubes. The van der Waals forces between adjacent CNTs will force all CNTs to growth to the free space and form the vertically-aligned mode (Figure 2b). Experimentally, once must optimize the growth parameters so that most catalyst particles remain active (see for examples in [12]). By doing so, dense bundles of CNTs can be grown as shown in Figure 2c either in single-, double-, or multi-walled structures [11].

VERTICALLY-ALIGNED BORON NITRIDE NANOTUBES

Boron nitride (BN) phases are structurally similar to those of carbon. For example, hexagonal-phase BN (h-BN) and cubic-phase BN (c-BN) are analogous to graphites and diamonds. In addition, BNNTs are structurally similar to carbon nanotubes (CNTs) and exhibit extraordinary mechanical properties. Despite these similarities, BNNTs are different from CNTs in other aspects. For example, BNNTs are having uniform electronic properties (band gap ~5.5 eV) that are insensitive to their diameters and chiralities [4, 5]. However, the synthesis of BNNTs is more challenging than that of CNTs. BNNTs were grown by arc discharge, laser ablation, substitution reactions from carbon nanotubes, ball-milling, and chemical vapor deposition (CVD) using reactive borazine, at temperatures from 1100 to 3000 °C (see comprehensive

references in [14]). BNNTs grown by these techniques are randomly oriented and dominated by impurities.

In 2005, we have succeeded for the first time on direct growth of *pure* BNNTs on substrates at 600 °C by a plasma-enhanced pulsed-laser deposition (PE-PLD) technique. The growth mechanism is schematically illustrated in Figure 3. In short, a negative substrate bias voltage induced by a nitrogen RF-plasma accelerates the positive ions in the RF plasma and the BN vapors to bombard on the substrate surface. When the kinetic energies of these ions are sufficient, the deposition rate of BN films is balanced by the rate of re-sputtering and result in total re-sputtering. The growth of BNNTs is highly reproducible under this condition. For example, for oxidized Si substrates with 12.5 nm thick Fe film, substrate bias voltages between zero to -300V will lead to the growth of BN films. At this condition, the deposition rate of BN films is faster than the diffusion rate of the BN growth species into the Fe catalyst nanoparticles. Thus thick BN films will be coated on the Fe catalyst and terminate the contact between Fe and the reactive growth species (Figure 3a). The thickness of BN films gradually reduces with an increase in the substrate bias (Figure 3b). BNNTs start to grow as a balance of film deposition rate and re-sputtering rate occurs at higher substrate bias (Figure 3c). At this total re-sputtering region (at a bias of ~ -380V in our case), the deposition of BN thin films is suppressed. BNNTs are grown on the Fe nanoparticles according to the VLS mechanism. The RF plasma creates a directional flux of the BN growth species with sufficient kinetic energies to diffuse into the Fe nanoparticles. Thus, Fe serves to capture the energetic BN growth species and confine them in a nanoscopic space. Otherwise, these species are re-sputtered off. When the Fe nanoparticles become supersaturated with BN vapor, the BN species condense into the ordered nanotubular structures. Groups of Fe nanoparticles will form vertical bundles of BNNTs as shown in Figure 3d. More recently, we reported that long and clean BNNTs can also be grown by thermal CVD just like growing CNTs [17].

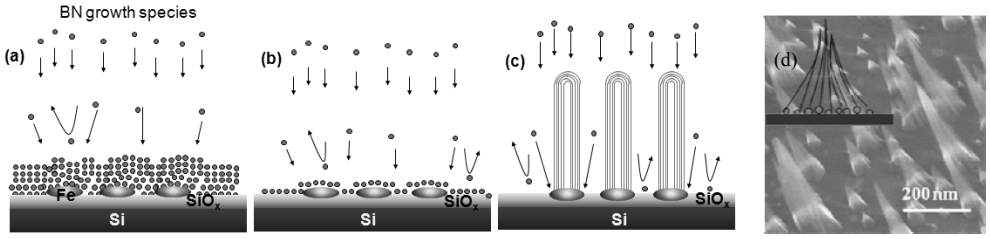

FIGURE 3. (a) At low bias volatges, deposition of thick BN films on Fe nanoparticles will occurred due to low re-sputtering rate of the growth species. (b) Reduced growth rate of BN films from energetic growth species induced by a higher substrate bias. (c) At a sufficient substrate bias, total re-sputtering region will be created where BNNTs are grown and BN films are totally re-sputtered and suppressed. (d) Bundles of BNNTs (schematic of the bundle as shown in the inset).

VERTICALLY-ALIGNED ZINC OXIDE NANOTUBES

Zinc oxide can appear in various nanostructures including nanowires, nanocombs, nanobelts and are popular for sensing applications [18]. Based on the theory of nucleation and vapor-solid crystal growth mechanism, we have experimentally

demonstrated direct growth of single crystalline ZnO nanotubes without the use of multiple processes, catalysts, or templates (see for comprehensive references in [6]). According to the theory of nucleation, the probability of nuclei formation is given by $P_N = N\exp(\frac{-\pi\sigma^2}{k^2T^2In\alpha})$, where σ is the surface energy, *α-1* is the supersaturation, $\alpha = p/p_o$, p is the pressure of vapor, p_o is the equilibrium vapor pressure of the condensed phase at that temperature, k is the Boltzmann constant, and T is the temperature in Kelvin. In addition, the binding energy of an ionic growth species (and generally for non-ionic growth species too) on a substrate is given by $E = \beta\frac{q^2}{a}$ [19], where β is a numerical factor which depends on the site of the deposition, a is the lattice spacing and q is the charge of the ion. These growth species prefer to condense on locations with the maximum number of nearest neighbors. Thus for a growth surface with a step as shown in Figure 4a, ions prefer to condense at sites 6, 5, 1, 4, 2, 3, according to sequence since $\beta_6 > \beta_5 > \beta_1 > \beta_4 > \beta_2 > \beta_3$. Thus an atomically flat layer will always spread from the edges under conditions with sufficient surface energy.

For an atomically flat 2D growth surface (without steps and defects), only site 1, 2, and 3 exist. In this case, higher binding energies at the edges (sites 1 and 2) will enable selective condensation of growth species at the edges. For ZnO, it is well known that the growth rate along the *c*-axis is relatively faster [20]. At decreased growth temperatures, the nucleation probability P_N , and the surface migration will be suppressed. Thus if the growth temperatures are low enough to suppress migration along the 2D surface of the c-plane but high enough to sustain the growth along the c-axis, the condensation and growth will be limited at the edges of the c-plane of ZnO as shown in Figure 4b. Under these conditions, the growth of ZnO nanotubes along the c-axis will be possible. However, if steps or vacancies are found in locations beyond the edges, nucleation will also take place at these sites as shown in Figure 4c due to their higher β values than those at the edges.

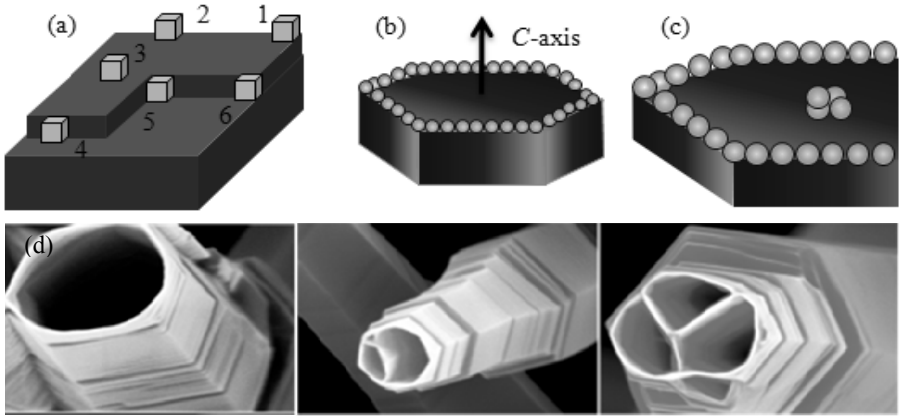

FIGURE 4. (a) Various nucleation sites on a surface with a step. (b) Preferential condensation of ZnO growth species at the edges of an atomically flat *c*-plane of a ZnO nanorod. (c) Addition nucleation beyond the edges will be formed when defects (steps, vacancies, etc.) are found. (d) Examples of ZnO nanotubes with single, double, and triple channels.

Based on this model, the growth of ZnO NTs were demonstrated experimentally by thermal CVD [6-8]. The diameters of these nanotubes are between 80 to 500 nm near the opened tips. As shown in Figure 4d, some of these nanotubes have single tubular channel as predicted by theory. Some of these nanotubes have multiple channels as also expected by the nucleation model discussed earlier.

ACKNOWLEDGMENTS

This work was supported by the U.S. Department of Army (Grant number W911NF-04-1-0029 through the City College of New York), National Science Foundation CAREER Award (Award number 0447555, Division of Materials Research), the Defense Advanced Research Projects Agency (Contract number DAAD17-03-C-0115 through the U.S. Army Research Laboratory), and the U. S. Department of Energy, the Office of Basic Energy Sciences (Grant No. DE-FG02-06ER46294).

REFERENCES

1. S. Iijima, *Nature* **354**, 56 (1991).
2. M. S. Dresselhaus and G. Dresselhaus, Eds., *Carbon Nanotubes: Synthesis, Structure, Properties and Applications*, Springer-Verlag, Berlin, 2001.
3. P. J. Harris, *Carbon Nanotubes and Related Structures*, Cambridge University Press, 2002.
4. A. Rubio, J. L. Corkill and M. L. Cohen, *Phys. Rev. B* **49**, 5081 (1994).
5. X. Blase, A. Rubio, S. G. Louie and M. L. Cohen, *Europhys. Lett.* **28**, 335 (1994).
6. S. L. Mensah, V. K. Kayastha, I. N. Ivanov, D. B. Geohegan and Y. K. Yap, *Appl. Phys. Letts.* **90**, 113108 (2007).
7. J. P. Moscatello, J. Wang, B. Ulmen, S. L. Mensah, M. Xie, S. Wu, A. Pandey, C. H. Lee, A. Prasad, V. K. Kayasha, and Y. K. Yap, in *Special Issue on Nanosensors for Defense & Security*, *IEEE Sensor Journal* **8**, 922 (2008).
8. S. L. Mensah, A. Prasad, J. Wang, and Y. K. Yap, in *A Special Section on Nanowires*, *J. Nanosci. Nanotechno*. **8**, 233 (2008).
9. M. Xie, J. Wang, Z. Fan, J. G. Lu, and Y. K. Yap, *Nanotechnology* **19**, 365609 (2008).
10. M. Xie, J. Wang, C. H. Lee, and Y. K. Yap, *Mater. Res. Soc. Symp. Proc.* Vol. **1057**, paper 1057-II13-03.
11. V. K. Kayastha, S. Wu, J. Moscatello, and Y. K. Yap, *J. Phys. Chem. C* (Letter) **111**, 10158 (2007).
12. V. Kayastha, Y. K. Yap, Z. Pan, I. Ivanov, A. A. Purezky, and D. B. Geohegan, *Appl. Phys. Lett.* **86**, 253105 (2005).
13. V. Kayastha, Y. K. Yap, S. Dimovski, and Y. Gogotsi, *Appl. Phys. Lett.* **85**, 3265 (2004).
14. J. Wang, V. Kayastha, Y. K. Yap, Z. Fan, J. G. Lu, Z. Pan, I. Ivanov, A. A. Purezky, and D. B. Geohegan, ," *Nano Lett.* **5**, 2528 (2005).
15. O. Kubaschewski, *Iron-binary phase diagram*, Springer-Verlag Berlin, 1982.
16. Z. L. Wang, J. M. Petroski, T. C. Green and M. A. El-Sayed, *J. Phys. Chem. B.* **102**, 6145 (1998).
17. C. H. Lee, J. Wang, V. K. Kayastha, J. Y. Huang, and Y. K. Yap, *Nanotechnology* **19**, 455605 (2008).
18. A. Prasad, S. Mensah, Z. W. Pan, Y. K. Yap, Chapter 4 - Alternative Nanostructured Sensors: Nanowires, Nanobelts, and Novel Nanostructures, in *Sensors Based on Nanostructured Materials*, Editor: Francisco J. Arregui, Springer, pg. 59-78 (2009).
19. I. Tarjan, M. Matrai, eds., *Laboratory Manual on Crystal Growth*, Akadémiai Kiadó, Budapest, 1972, pp 29-30.
20. Y. Li, G. W. Meng, L. D. Zhang and F. Phillipp, *Appl. Phys. Lett.* **76**, 2011 (2000).